www.ietdl.org

Published in IET Communications
Received on 25th November 2012
Revised on 29th January 2013
Accepted on 2nd March 2013
doi: 10.1049/iet-com.2012.0731

ISSN 1751-8628

Practical linear precoder design for finite alphabet multiple-input multiple-output orthogonal frequency division multiplexing with experiment validation

Yahong Rosa Zheng, Mingxi Wang, Weiliang Zeng, Chengshan Xiao

Department of Electrical and Computer Engineering, Missouri University of Science and Technology, Rolla, MO 65409, USA
E-mail: xiaoc@mst.edu

Abstract: A low complexity precoding method is proposed for practical multiple-input multiple-output (MIMO) orthogonal frequency-division multiplexing (OFDM) systems. Based on the two-step optimal precoder design algorithm that maximises the lower bound of the mutual information with finite-alphabet inputs, the proposed method simplifies the precoder design by fixing the right singular vectors of the precoder matrix, eliminating the iterative optimisation between the two steps, and discretising the search space of the power allocation vector. For a 4×4 channel, the computational complexity of the proposed precoder design is reduced to 3 and 6% of that required by the original two-step algorithm with quadrature phase shift keying (QPSK) and 8 phase-shift keying (***8PSK***), respectively. The proposed method achieves nearly the same mutual information as the two-step iterative algorithm for a large range of signal-to-noise ratio (SNR) region, especially for large MIMO size and/or high constellation systems. The proposed precoding design method is applied to a 2×2 MIMO-OFDM system with 2048 subcarriers by designing 1024 precoders for extended channel matrices of size 4×4. A transceiver test bed implements these precoding matrices in comparison with other existing precoding schemes. Indoor experiments are conducted for fixed-platform non-line-of-sight channels, and the data processing results show that the proposed precoding method achieves the lowest bit error rate compared with maximum diversity, classic water-filling and channel diagonalisation methods.

1 Introduction

Linear precoding for multiple-input multiple-output (MIMO) communications has been a popular research topic in the last decade. Traditional precoding methods include maximising the channel capacity with Gaussian inputs [1], maximising the diversity order [2], maximising the signal to interference-plus-noise ratio (SINR) [3], minimising the mean square error (MSE) [3] etc. More recently, several works have found that designing precoders by maximising mutual information with finite-alphabet inputs can achieve higher mutual information [4–10] and lower bit error rate (BER) [11] than employing other optimisation criteria. The performance benefits of these approaches [4–11] come from optimisation of mutual information with finite-alphabet input constraints, compared with using other indirect methods such as maximising channel capacity with Gaussian inputs, maximising diversity order, minimising SINR or minimising MSE.

However, applying precoding to practical MIMO systems encounter a few obstacles. First of all, the algorithms developed to find the optimal precoders [10–14] are computationally complicated because of their iterative algorithm and multiple computations of gradients through Monte-Carlo simulations. For instance, Pérez-Cruz *et al.* [10] utilised the gradient descent algorithm to directly find the precoding matrix, and [14] proposed a two-step iterative algorithm to exploit the precoder structure. Even offline calculation of precoders is prohibitive for large MIMO dimensions and high constellations. Second, the soft maximum *a posteriori* probability (MAP) detector [15] is often employed for performance evaluation [11, 12] and good BER performance have been demonstrated. However, MAP-based iterative receiver has the highest complexity and is thus difficult to implement in practice. Whether the performance gain of precoders can be leveraged by practical suboptimal receivers is still questionable. In addition, the demonstrated performance gains in [5–14] are all based on simulations over either fixed channels or statistical models of fading channels. The feasibility of employing precoders in practical communication systems and their performances under real-world wireless channels are rarely studied.

In this paper, we first propose a low complexity precoding design method to simplify the two-step precoder design algorithm that maximises the lower bound of the mutual information with finite-alphabet inputs [14]. The proposed method employs fixed right singular vectors that are modulation diversity matrices designed for different modulation schemes; thus, eliminating the need for iterative optimisation between two steps – one for the right singular vectors, one for the power allocation vector. Furthermore, the proposed method discretises the search space of the

power allocation vector and further reduces the complexity of the iterative design of the power allocation. For a 4×4 channel, the computational complexity of the proposed precoder design is reduced to 3 and 6% of that required by the two-step algorithm for quadrature phase shift keying (QPSK) and ***8PSK***, respectively. Moreover, the proposed method achieves nearly the same mutual information as the original two-step iterative algorithm for a large range of SNR region for high constellation or under large-sized MIMO channels. It also outperforms the maximum diversity, classic water-filling and channel diagonalisation methods in a large region of SNR.

The proposed precoding design method is applied to a 2×2 MIMO-orthogonal frequency-division multiplexing (OFDM) system with 2048 subcarriers for QPSK, ***8PSK*** and 16 quadrature amplitude modulation (QAM). For each modulation scheme, we design 1024 precoders for the extended channel matrices of size 4×4 that combines the 2×2 MIMO with two subcarriers, thus leveraging frequency diversity gain along spatial diversity gains. Moreover, the precoders are designed for one specified SNR value that applies to a range of practical SNR values will not only reduce the computational cost further, but also meet the practical requirement on precoder designs.

The designed precoding matrices are implemented in a field programable gate array (FPGA)-based transceiver test bed employing a rate 3/4 low-density parity-check (LDPC) code, where the baseband transmitter and digital intermediate frequency (IF) circuits are implemented in Altera's Stratix III FPGA. Two baseband receiver algorithms are realised: the soft minimum mean square error (MMSE) linear equaliser with interference cancelation [16, 17] in Altera's Stratix IV FPGA, and the fixed-complexity list sphere decoding (FSD) algorithm [18, 19] in MATLAB. Although various MIMO-OFDM testbeds [20–26] are reported in the literature for wideband communications, they focus mainly on supporting spatial multiplexing [21–25] and transmit diversity schemes [20] or space time block codes [21, 23] or polarisation diversity [26]. To the best of our knowledge, this is the first test bed that implements precoder designs in the transmitter and the corresponding iterative detection in the receiver.

With the MIMO-OFDM test bed, we conduct indoor non-line-of-sight (NLOS) experiment to acquire channels, design precoders offline, and verify performance with precoding. The data processing results of the experiments show that the proposed precoding method achieves the lowest BER compared with maximum diversity, classic water-filling and channel diagonalisation methods. Besides, the maximum diversity outperforms the classic water-filling and channel diagonalisation methods.

Throughout the paper, we denote vectors with boldface lower-case letters and matrices with boldface upper-case letters. The superscripts $(\cdot)^h$ and $(\cdot)^+$ represent conjugate transpose and pseudoinverse operations, respectively. In addition, the symbol $\mathbb{C}$ stands for the complex number field, and diag$\{\boldsymbol{a}\}$ denotes a diagonal matrix with elements of vector $\boldsymbol{a}$.

2 Linear precoder design for finite-alphabet

Consider a MIMO system with baseband equivalent model

$$\boldsymbol{y} = \boldsymbol{HGx} + \boldsymbol{n} \tag{1}$$

where the vector $\boldsymbol{x} \in \mathbb{C}^{N_i \times 1}$ contains transmitted signals of N_i symbols. The matrix $\boldsymbol{H} \in \mathbb{C}^{N_o \times N_i}$ is the complex channel matrix, and $\boldsymbol{G} \in \mathbb{C}^{N_i \times N_i}$ is the designed precoding matrix. The receiver noise $\boldsymbol{n} \in \mathbb{C}^{N_o \times 1}$ is a zero mean circularly symmetric complex Gaussian vector with covariance matrix $\sigma^2\boldsymbol{I}$, that is, $\boldsymbol{n} \sim \mathcal{CN}(\boldsymbol{0}, \sigma^2\boldsymbol{I})$.

To design the precoding matrix $\boldsymbol{G}$, we first decompose the channel matrix $\boldsymbol{H}$ via singular value decomposition (SVD), thus

$$\boldsymbol{H} = \boldsymbol{U}_{\boldsymbol{H}} \sum_{\boldsymbol{H}} \boldsymbol{V}_{\boldsymbol{H}}^h \tag{2}$$

where $\boldsymbol{U}_{\boldsymbol{H}}$ and $\boldsymbol{V}_{\boldsymbol{H}}$ are unitary matrices, and $\boldsymbol{\Sigma}_{\boldsymbol{H}}$ is a diagonal matrix.

Similarly, the precoding matrix $\boldsymbol{G}$ can also be decomposed into three components as

$$\boldsymbol{G} = \boldsymbol{U}_{\boldsymbol{G}} \sum_{\boldsymbol{G}} \boldsymbol{V}_{\boldsymbol{G}}^h \tag{3}$$

in which $\boldsymbol{U}_{\boldsymbol{G}}$ and $\boldsymbol{V}_{\boldsymbol{G}}$ are left and right singular vectors of $\boldsymbol{G}$, respectively. The diagonal matrix $\boldsymbol{\Sigma}_{\boldsymbol{G}}$ has all singular values. The decomposition in (3) is a general form that incorporates the four precoding schemes we discuss in this paper.

Scheme 1 is the channel diagonalisation precoder, also known as parallel decomposition [27, 28], which sets $\boldsymbol{V}_{\boldsymbol{G}}$ and $\boldsymbol{\Sigma}_{\boldsymbol{G}}$ to identity matrices, and $\boldsymbol{U}_{\boldsymbol{G}} = \boldsymbol{V}_{\boldsymbol{H}}$. The precoding matrix is then given by

$$\boldsymbol{G}_{\boldsymbol{D}} = \boldsymbol{V}_{\boldsymbol{H}} \tag{4}$$

which simply diagonalises the channel.

Scheme 2 is the classic water-filling precoder which maximises the channel capacity assuming that the input signal $\boldsymbol{x}$ is Gaussian distributed. The MIMO channel capacity with Gaussian input assumption is [27]

$$C = \max_{\mathrm{Tr}(\boldsymbol{Q})=\mathrm{P}} \log\left|\boldsymbol{I} + \frac{1}{\sigma^2}\boldsymbol{H}\,\boldsymbol{Q}\,\boldsymbol{H}^h\right| \tag{5}$$

where P is the transmit power and $\boldsymbol{Q}$ is the covariance matrix after precoding, such that

$$\boldsymbol{Q} = \boldsymbol{V}_{\boldsymbol{H}} \sum_{\boldsymbol{WF}} \boldsymbol{V}_{\boldsymbol{H}}^h \tag{6}$$

where the diagonal matrix $\boldsymbol{\Sigma}_{\boldsymbol{WF}}$ (subscript bold and italic) can be solved by water-filling [1, 27]. Since $\boldsymbol{Q} = \boldsymbol{G}\boldsymbol{G}^h$, the classic water-filling precoding matrix is

$$\boldsymbol{G}_{\boldsymbol{WF}} = \boldsymbol{V}_{\boldsymbol{H}} \sum_{\boldsymbol{WF}}^{(1/2)} \tag{7}$$

Scheme 3 is the maximum diversity precoder, which maximises the diversity order for two-dimensional constellations without Gaussian input assumptions [2]. It consists of two matrices in (3)

$$\boldsymbol{G}_{\boldsymbol{MD}} = \boldsymbol{V}_{\boldsymbol{H}}\boldsymbol{V}_{\boldsymbol{MD}} \tag{8}$$

in which $\boldsymbol{V}_{\boldsymbol{MD}}$ is a matrix obtained through the algebraic construction and it is designed to be the same for all types of modulations. Specifically, when N_i is a power of two,

$\boldsymbol{V}_{\boldsymbol{MD}}$ is a unitary matrix given by

$$\boldsymbol{V}_{\boldsymbol{MD}} = \frac{1}{\sqrt{N_i}} \begin{bmatrix} 1 & \alpha_1 & \dots & \alpha_1^{N_i-1} \\ 1 & \alpha_2 & \dots & \alpha_2^{N_i-1} \\ \vdots & \vdots & & \vdots \\ 1 & \alpha_{N_i} & \dots & \alpha_{N_i}^{N_i-1} \end{bmatrix} \tag{9}$$

in which

$$\alpha_k = \exp\left[\mathrm{j}\pi \frac{4(k-1)+1}{2N_i}\right], \quad k = 1, 2, \dots, N_i \tag{10}$$

Scheme 4 is the optimal precoding, which maximises the channel mutual information directly with finite-alphabet inputs. Based on the signal model in (1), the mutual information between the input $\boldsymbol{x}$ and output $\boldsymbol{y}$ is given by [11]

$$\mathcal{I}(\boldsymbol{H}, \boldsymbol{G}) = N_i \log M - \frac{1}{M^{N_i}} \sum_{m=1}^{M^{N_i}} E_{\boldsymbol{n}} \left[\log \sum_{k=1}^{M^{N_i}} \exp\left(-d_{\mathrm{mk}}\right) \right] \tag{11}$$

where $d_{\mathrm{mk}} = (\|\boldsymbol{HG}\boldsymbol{e}_{\mathrm{mk}} + \boldsymbol{n}\|^2 - \|\boldsymbol{n}\|^2)/\sigma^2$, and $\boldsymbol{e}_{\mathrm{mk}} = \boldsymbol{x}^m - \boldsymbol{x}^k$. The symbol $E_{\boldsymbol{n}}[\cdot]$ takes expectation over the noise $\boldsymbol{n}$. The signal $\boldsymbol{x}^m$ is a vector with each of its elements drawn from the M-ary signal constellation.

The calculation of the mutual information in (11) involves mathematical expectation, which is often estimated through Monte Carlo simulations [10] that is computationally expensive. To reduce the high computational complexity caused by Monte Carlo simulations of the expectation, a lower bound of mutual information is derived in [29] as

$$\mathcal{I}_L(\boldsymbol{H}, \boldsymbol{G}) = N_i \log M - \left(1/\ln 2 - 1\right) N_{\mathrm{o}} - \frac{1}{M^{N_i}} \sum_{m=1}^{M^{N_i}} \log \sum_{k=1}^{M^{N_i}} \exp\left(- \frac{\boldsymbol{c}_{\mathrm{mk}}^H \boldsymbol{c}_{\mathrm{mk}}}{2\sigma^2} \right) \tag{12}$$

where N_{o} is the number of received antennas as indicated in the first paragraph of Section 2, and $\boldsymbol{c}_{\mathrm{mk}} = \boldsymbol{HG}(\boldsymbol{x}^m - \boldsymbol{x}^k)$. It is shown that the lower bound (12) with a constant shift is an accurate approximation of the mutual information (11) under various channel conditions [29].

Employing this lower bound and setting $\boldsymbol{U}_{\boldsymbol{G}} = \boldsymbol{V}_{\boldsymbol{H}}$ in the precoder design yields a two-step iterative algorithm [14]. After initialisations, the algorithm alternatively updates $\boldsymbol{\Sigma}_{\boldsymbol{G}}$ and $\boldsymbol{V}_{\boldsymbol{G}}$ in the two steps until the convergence. During each iteration, the first step is to optimise the power allocation vector $\boldsymbol{1} = \mathrm{diag}(\boldsymbol{\Sigma}_{\boldsymbol{G}})$ given $\boldsymbol{V}_{\boldsymbol{G}}$

$$\text{maximise} \quad \mathcal{I}_L(\boldsymbol{\lambda}) \tag{13}$$

$$\text{subject to} \quad \boldsymbol{1}^{\mathrm{T}}\boldsymbol{\lambda} = N_i \tag{14}$$

$$\boldsymbol{\lambda} \succeq \boldsymbol{0} \tag{15}$$

where $\mathcal{I}_L(\boldsymbol{\lambda})$ is the lower bound in (12). Given the $\boldsymbol{\lambda}$ obtained in the first step, the second step is to optimise $\boldsymbol{V}_{\boldsymbol{G}}$

$$\text{maximise} \quad \mathcal{I}_L(\boldsymbol{V}_{\boldsymbol{G}}) \tag{16}$$

$$\text{subject to} \quad \boldsymbol{V}_{\boldsymbol{G}}^h \boldsymbol{V}_{\boldsymbol{G}} = \boldsymbol{I} \tag{17}$$

As shown later in Section 3, the computational complexity of the optimal precoder design using the lower bound is still prohibitively high. Moreover, the complexity grows exponentially with the modulation level M and the size of precoding matrix N_i. Thus, lowering the overall computational complexity further is necessary to make practical use of the precoder design.

3 Proposed simplified linear precoder design for finite-alphabet

To reduce the complexity of the precoder design, we propose a non-iterative approach to design precoder for finite-alphabet inputs. The proposed precoder $\boldsymbol{G}$ contains three components as follows

$$\boldsymbol{G} = \boldsymbol{V}_{\boldsymbol{H}} \sum_{\boldsymbol{G}} \boldsymbol{V}_{\mathrm{mod}} \tag{18}$$

where $\boldsymbol{V}_{\boldsymbol{mod}}$ is a unitary matrix designed for different modulation constellations and it is referred to as modulation diversity matrix in this paper. The matrix $\boldsymbol{\Sigma}_{\boldsymbol{G}}$ is a diagonal matrix for power allocation policy depending on both the channel condition and modulation constellation. The non-iterative precoder design approach first fixes $\boldsymbol{V}_{\boldsymbol{mod}}$ and then solves $\boldsymbol{\Sigma}_{\boldsymbol{G}}$.

The modulation diversity matrix $\boldsymbol{V}_{\boldsymbol{mod}}$ in (18) is different from the maximum diversity matrix [2], because $\boldsymbol{V}_{\boldsymbol{mod}}$ is tailored for the constellation used for the transmitted signal vector $\boldsymbol{x}$. Specifically, we propose the following structure for the design of the modulation diversity matrix

$$\boldsymbol{V}_{\boldsymbol{mod}} = \frac{1}{\sqrt{N_i}} \begin{bmatrix} 1 & \beta_1 & \dots & \beta_1^{N_i-1} \\ 1 & \beta_2 & \dots & \beta_2^{N_i-1} \\ \vdots & \vdots & & \vdots \\ 1 & \beta_{N_i} & \dots & \beta_{N_i}^{N_i-1} \end{bmatrix} \tag{19}$$

where

$$\beta_k = \exp\left[j\pi \frac{2(k-1)+q_{\boldsymbol{mod}}}{N_i}\right], \quad k = 1, 2, \dots, N_i \tag{20}$$

where the transmit antenna number N_i can be any positive integer.

The parameter $q_{\boldsymbol{mod}}$ is a rotation angle depending on the modulation type. For M-PSK modulations, $q_{\boldsymbol{mod}}$ is $(1/2)^{M-1}$, where M is the constellation size. The rotation angle $q_{\boldsymbol{mod}}$ is (1/2) for all QAM such as 4, 16 and 64QAMs. Table 1 lists values of $q_{\boldsymbol{mod}}$ for different modulations. The key criterion to choose $q_{\boldsymbol{mod}}$ is to maximise the constellation expansion for the precoded signal vector as demonstrated in Fig. 1 that will be depicted and explained a bit later.

Actually, the modulation diversity matrix for 2×2 MIMO system can be easily derived from the values of ν of Table 1 in [11]. The corresponding modulation diversity matrix for 4×4 MIMO system can be obtained with the extension of 2×2 MIMO systems.

Comparing (20) and (10), we see that the modulation diversity matrix is identical to the maximum diversity for QAM and QPSK modulations when N_i is a power of two. However, these two methods are different from each other for other modulations, and/or for the case when N_i is not a power of two. For instance, the 2×2 maximum diversity

doi: 10.1049/iet-com.2012.0731

Table 1 Values of q_{mod} corresponding to different modulations

Modulation	***BPSK***	QPSK	***8PSK***	16PSK	16QAM	64QAM
q_{mod}	1	$\frac{1}{2}$	$\frac{1}{4}$	$\frac{1}{8}$	$\frac{1}{2}$	$\frac{1}{2}$

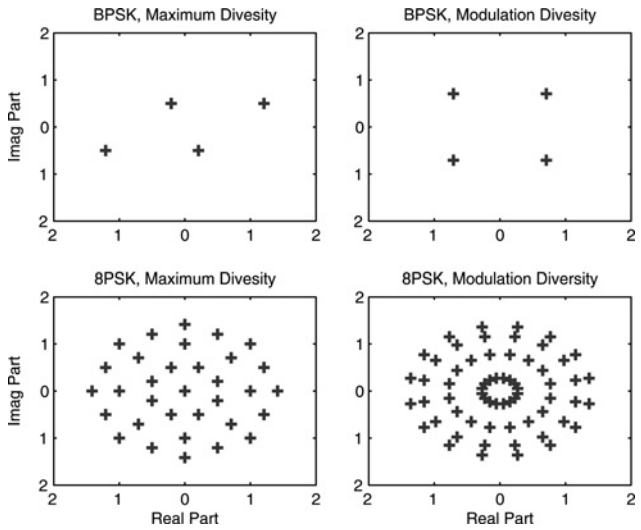

Fig. 1 *Scatter plot of the precoded **BPSK** and **8PSK** signals using 2 × 2 maximum diversity and modulation diversity*

matrix for all types of modulations is given by

$$\boldsymbol{V}_{\boldsymbol{MD}} = \frac{1}{\sqrt{2}}\begin{bmatrix} 1 & e^{j(\pi/4)} \\ 1 & e^{j(5\pi/4)} \end{bmatrix} \tag{21}$$

On the other hand, the 2 × 2 modulation diversity matrices for binary phase shift keying (***BPSK***) and ***8PSK*** modulations are

$$\begin{aligned} \boldsymbol{V}_{\boldsymbol{mod-BPSK}} &= \frac{1}{\sqrt{2}}\begin{bmatrix} 1 & e^{j(\pi/2)} \\ 1 & e^{j(3\pi/2)} \end{bmatrix}, \\ \boldsymbol{V}_{\boldsymbol{mod-8PSK}} &= \frac{1}{\sqrt{2}}\begin{bmatrix} 1 & e^{j(\pi/8)} \\ 1 & e^{j(9\pi/8)} \end{bmatrix} \end{aligned} \tag{22}$$

For QPSK and 16QAM modulations, the modulation diversity matrices are the same as the maximum diversity matrix.

In Fig. 1, we plot the constellations of precoded ***BPSK*** and ***8PSK*** inputs using 2 × 2 modulation and maximum diversity matrices. It can be seen that the scatter plot of the modulation diversity for ***BPSK*** inputs is the same as the QPSK constellation, which is different from the result obtained by maximum diversity. Comparing with the scatter plots of ***8PSK*** inputs, we note that there are 33 and 64 points for maximum and modulations diversity, respectively. This indicates that one of the shortcomings of the maximum diversity is that the original 64 possible signal points in $\boldsymbol{x}$ collapse to less points in the scatter plot after precoding. The modulation diversity, on the other hand, preserves all the signal points in the constellations and converts them to a complex Gaussian-like scatter plot.

After $\boldsymbol{V}_{\boldsymbol{mod}}$ is fixed, $\boldsymbol{\Sigma}_{\boldsymbol{G}}$ can be found by exhaustive search based on the lower bound of the mutual information. Specifically, we partition [0, 1] into K uniform segments. Assume that the diagonal matrix $\boldsymbol{\Sigma}_{\boldsymbol{G}} = \text{diag}\{\sigma_1, \ldots, \sigma_{Ni}\}$ and each σ_i is chosen from the set $\{0, (1/K), (2/K), \ldots, (K/K)\}$. Thus, there are totally $(K+1)^{N_i}$ combinations for all the N_i diagonal elements in $\boldsymbol{\Sigma}_{\boldsymbol{G}}$. For each combination of $\{\sigma_1, \ldots, \sigma_{N_i}\}$, we normalise their values as $\tilde{\sigma}_i = \sigma_i\sqrt{N_i}/\sum_{i=1}^{N_i}|\sigma_i|^2$, so that the power of the resulting precoding matrix $\boldsymbol{G}$ is N_i. Each normalised diagonal matrix $\boldsymbol{\Sigma}_{\boldsymbol{G}^k}$ along with the fixed $\boldsymbol{V}_{\boldsymbol{mod}}$ corresponds to a precoding matrix $\boldsymbol{G}^k = \boldsymbol{V}_{\boldsymbol{H}}\boldsymbol{\Sigma}_{\boldsymbol{G}^k}\boldsymbol{V}_{\text{mod}}$. By computing the lower bound of $\mathcal{I}_L(\boldsymbol{H}, \boldsymbol{G}^k)$, $k = 1, \ldots, (K+1)^{N_i}$, and choosing the $\boldsymbol{G}^k$ with the maximum lower bound, we find the approximate optimal precoder. We note that the proposed discretisation of the power allocation diagonal matrix can be viewed as an extension to the well known on/off power allocation technique [30].

From the aforementioned procedure, we note that the proposed simplified precoding is a non-iterative method. Moreover, it avoids the computation of the derivative of $\mathcal{I}_L(\boldsymbol{H}, \boldsymbol{G})$ that is more time consuming than computing $\mathcal{I}_L(\boldsymbol{H}, \boldsymbol{G})$ itself, especially when the size of the precoding matrix N_i is large. Therefore the proposed method has a lower complexity than the two-step iterative algorithm in [14].

To verify the complexity and performance merits of the proposed precoders, we consider a constant 2 × 2 channel and a complex 4 × 4 channel

$$\boldsymbol{H}_1 = \begin{bmatrix} 2 & 1 \\ 1 & 1 \end{bmatrix} \tag{23}$$

and (see (24)) in which the 2 × 2 channel $\boldsymbol{H}_1$ is also used in [4, 11, 14]. The SNR is defined as $\text{SNR}_i = \text{Tr}(\boldsymbol{H}_i\boldsymbol{H}_i^h)/(N_o\sigma^2)$, for $i = 1, 2$, [11].

Table 2 lists the central processing unit (CPU) time of obtaining precoders using two-step iterative algorithm [14] and the proposed method for the 4 × 4 channel $\boldsymbol{H}_2$. The codes for both methods are mostly written in MATLAB, except that the part of computing lower bound $\mathcal{I}_L(\boldsymbol{H}, \boldsymbol{G})$ is implemented in C++. The simulations are executed on an Intel E8600 3.33 GHz duo core processor. In the proposed method, K is set to be 4. Thus, the total number of calculated lower bounds is $5^4 = 625$. The results in Table 2 show that the proposed method consumes much less time than the two-step iterative algorithm for QPSK and ***8PSK***

$$\boldsymbol{H}_2 = \begin{bmatrix} 0.1897 + 0.6602i & 0.5417 + 0.5341i & 0.8600 + 0.5681i & 0.8998 + 0.4449i \\ 0.1934 + 0.3420i & 0.1509 + 0.7271i & 0.8537 + 0.3704i & 0.8216 + 0.6946i \\ 0.6822 + 0.2897i & 0.6979 + 0.3093i & 0.5936 + 0.7027i & 0.6449 + 0.6213i \\ 0.3028 + 0.3412i & 0.3784 + 0.8385i & 0.4966 + 0.5466i & 0.8180 + 0.7948i \end{bmatrix} \tag{24}$$

Table 2 CPU time, s of designing precoders for the 4 × 4 channel $\boldsymbol{H}_2$

SNR, dB	QPSK		*8PSK*	
	Two-step iterative algorithm	Proposed method	Two-step iterative algorithm	Proposed method
−10	177.3064	3.0144	19 655	743.6521
−5	163.5079	3.0518	10 885	753.4039
5	82.2510	3.0593	11 692	755.4079
10	106.9154	3.0773	12 707	755.8201
15	178.5296	3.1564	12 204	779.5273

modulations under various SNRs. For example, when SNR = 10 dB, the CPU time of running the proposed method for QPSK and ***8PSK*** modulations is about 3 and 6% that of the two-step iterative algorithm, respectively.

The mutual information results of different modulations for channel $\boldsymbol{H}_1$ and $\boldsymbol{H}_2$ are shown in Fig. 2a – f, where for comparison purpose, maximum diversity, classic water-filling and channel diagonalisation are also provided. For the 2 × 2 channel with QPSK and ***8PSK*** inputs, the proposed method performs almost the same as the two-step iterative algorithm in the low and medium SNR regions. As the SNR increases, its performance becomes apart from the two-step iterative algorithm, but still better than that of the maximum diversity method. On the other hand, it is seen from Fig. 2c–e that the proposed method and the two-step iterative algorithm have nearly the same performances for a large range of SNR region under the 2 × 2 channel with 16QAM inputs, and the 4 × 4 channel with QPSK and ***8PSK*** inputs. Owing to the extremely high computational complexity, the two-step iterative algorithm has not been simulated for the 4 × 4 channel with 16QAM inputs. Yet, Fig. 2*f* shows that the proposed method achieves higher mutual information than the maximum diversity for the 16QAM. In all cases, the proposed method performs better than the classic water-filling and channel diagonalisation methods especially in the medium and high SNR regions.

Remark: before proceeding further, we would like to explain why the proposed method can perform better than other algorithms as shown in Fig. 2. As we know, based on the previous discussions, the four different algorithms have different precoder structures as shown in Table 3, in which we also list the corresponding precoder solutions for $\boldsymbol{H}_1$ at SNR = 3 dB. The solution structures tell us that for each transmitted signal vector $\boldsymbol{x} = [x_1, x_2]^t$, the classic water-filling solution $\boldsymbol{G}_{\boldsymbol{WF}}$ will throw away x_2 and only transmits x_1. In other words, every two symbols, the transmitter only sends one symbol and deletes the other symbol. However, our proposed method $\boldsymbol{G}_{\boldsymbol{o}}$ will use the right singular vectors to combine both x_1 and x_2, resulting in $\theta_{11}x_1 + \theta_{12}x_2$, and then transmit it. It does not throw away (finite-alphabet) information symbols, and it includes the power allocation policy. For the 'Channel Diagonalisation' and 'Maximum Diversity' methods, they do not throw away information symbols but they do not have power allocation policy either. These are the main reasons that our proposed approach can perform better than other methods.

To leverage the benefit of precoding in practical MIMO-OFDM systems, we further propose to apply linear precoding to extended channel matrices that combine $N_r \times N_t$ MIMO and K_G subcarriers. Specifically, we divide the total of N_f subcarriers into N_g groups and perform linear precoding for the extended $(N_r \cdot K_G) \times (N_t \cdot K_G)$ channel in each group. For example, when $N_t = 2$, $N_t = 2$, $K_G = 2$ and $N_f = 2048$, precoders of size 4 × 4 are designed for 1024 groups. We group the symbols from the two subcarriers and two transmitted data streams to a 4 × 1 column vector as the equivalent channel input. Each signal vector is then multiplied by the 4 × 4 linear precoding matrix. By using a larger size precoder, higher precoding gain can be achieved than that of precoding without the subcarrier grouping.

In addition, an interleaver is employed for the subcarrier grouping so that each interleaved group contains both statistically strong and weak frequency tones; thus, the diversity gain is achieved by leveraging both spatial and frequency correlation of the MIMO channels. To illustrate this, we assume that $\boldsymbol{H}_k$ represents the k-th frequency tone of all the channel matrices, the matrix $\boldsymbol{H}_k$ has the same distribution as $\sqrt{f_k}\boldsymbol{\Psi}_{\mathrm{RX}}^{(1/2)}\boldsymbol{H}_{w,k}\boldsymbol{\Psi}_{\mathrm{RX}}^{(1/2)}$ [31] for Rayleigh fading, where $\boldsymbol{\Psi}_{\mathrm{RX}}$ and $\boldsymbol{\Psi}_{\mathrm{TX}}$ are the antenna spatial correlation matrices because of angle spreads at the transmitter and receiver, respectively. The matrix $\boldsymbol{H}_{w,k}$ is an $N_r \times N_t$ random matrix with i.i.d $\sim \mathcal{CN}(0, 1)$ elements. The scalar f_k is the channel spectrum function given by

$$f_k = 1 + 2\sum_{i=1}^{L-1} a_i \cos\left[\frac{2\pi i(k-0.5)}{N_f}\right], \quad k = 1, \ldots, N_f \tag{25}$$

and

$$a_i = \sum_{l=1}^{L-i} \boldsymbol{\Psi}_{\mathrm{ISI}}(l,\ l+i) \tag{26}$$

in which $\boldsymbol{\Psi}_{\mathrm{ISI}}$ is the inter-tap correlation matrix [32]. The average power of the kth frequency tone is

$$\mathrm{Tr}\left[E\left(\boldsymbol{H}_k\boldsymbol{H}_k^h\right)\right] = f_k \times \mathrm{Tr}\left(\boldsymbol{\Psi}_{\mathrm{RX}}\right) \times \mathrm{Tr}\left(\boldsymbol{\Psi}_{\mathrm{RX}}\right) \tag{27}$$

According to (25) and (26), the low-frequency tones (when k is small) have stronger average power than the high-frequency tones (when k is around $N_f/2$). Thus, the objective of the interleaver is that the interleaved frequency tones in different groups have similar descending patterns on the average power.

Fig. 3 gives an example indicating the effect of subcarrier grouping for a 2 × 2 MIMO-OFDM system. For comparison, signals without subcarrier grouping are shown in Fig. 3*a*. In Fig. 3*b*, each group has signals from two subcarriers, that is $K_G = 2$. It is seen that each group contains strong and weak signals when interleaving is employed in the subcarrier grouping.

4 Applications of linear precoding to MIMO-OFDM system

In this section, we present the MIMO-OFDM system that employs the designed 4 × 4 linear precoding matrices for verification purposes. Specifically, we will discuss the data frame structure, system diagram and receiver algorithms.

The system diagram of the 2 × 2 MIMO-OFDM testbed is shown in Fig. 4, where the transmitter employs a signaling frame structure shown in Fig. 5. The 144-bit ***BPSK***

doi: 10.1049/iet-com.2012.0731

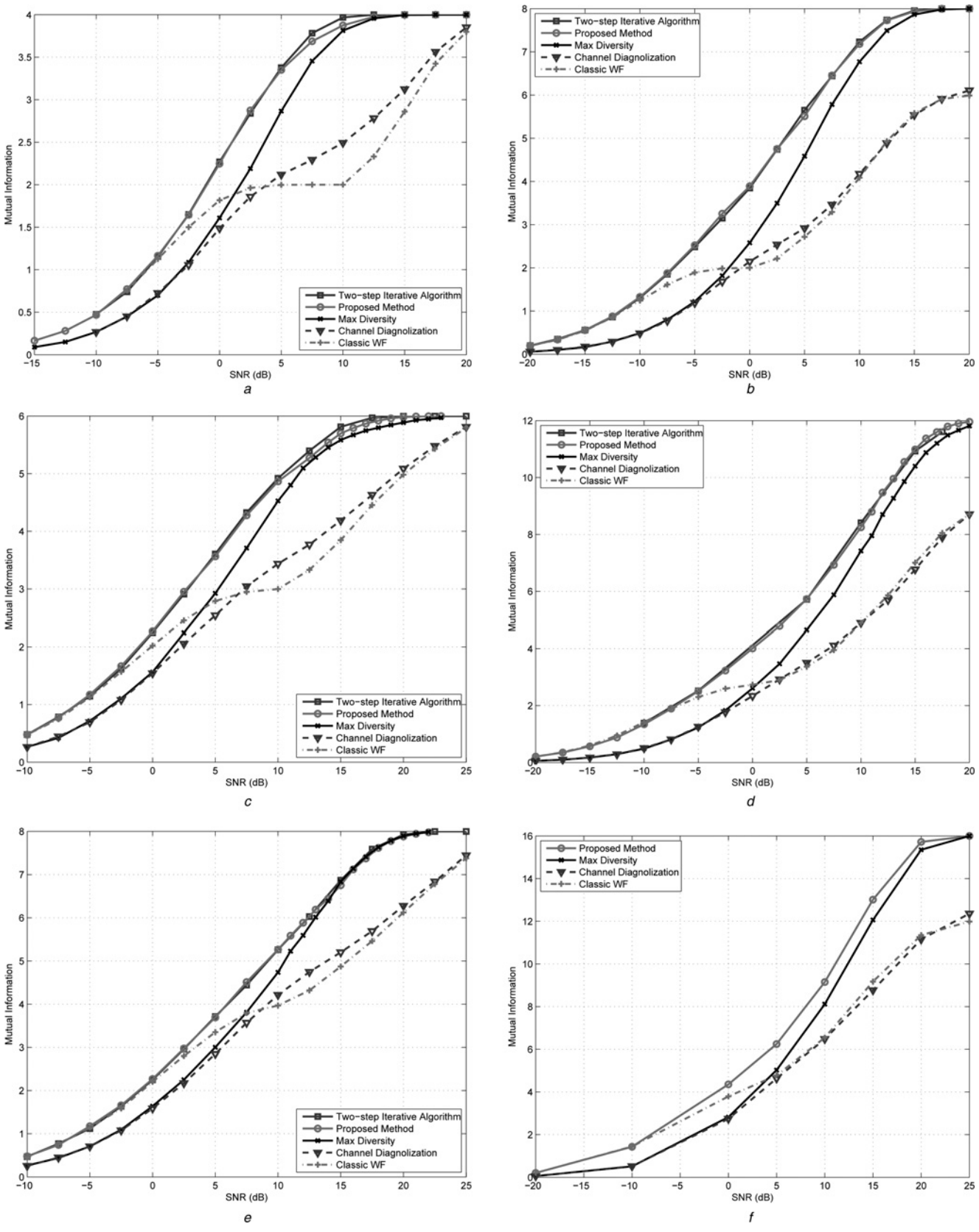

Fig. 2 *Mutual information against SNR*

a 2 × 2 Channel with QPSK inputs
b 4 × 4 Channel with QPSK inputs
c 2 × 2 Channel with 8PSK inputs
d 4 × 4 Channel with 8PSK inputs
e 2 × 2 Channel with 16QAM inputs
f 4 × 4 Channel with 16QAM inputs

Table 3 Linear precoder structures and corresponding solutions for H_1 at SNR = 3 dB

Scheme	Channel diagonalisation	Classic water-filling	Maximum diversity	Proposed method
structure	$G_D = V_H$	$G_{WF} = V_H \Sigma_{WF}^{1/2}$	$G_{MD} = V_H V_{MD}$	$G_o = V_H \Sigma_G V_{mod}$
solution at SNR = 3 dB	$G_D = V_H$	$G_{WF} = V_H \begin{bmatrix} \sqrt{2} & 0 \\ 0 & 0 \end{bmatrix}$	$G_{MD} = V_H V_{MD}$	$G_o = V_H \begin{bmatrix} \sqrt{2} & 0 \\ 0 & 0 \end{bmatrix} \begin{bmatrix} \theta_{11} & \theta_{12} \\ \theta_{21} & \theta_{22} \end{bmatrix}$
comment	no power allocation	with power allocation	no power allocation	with power allocation

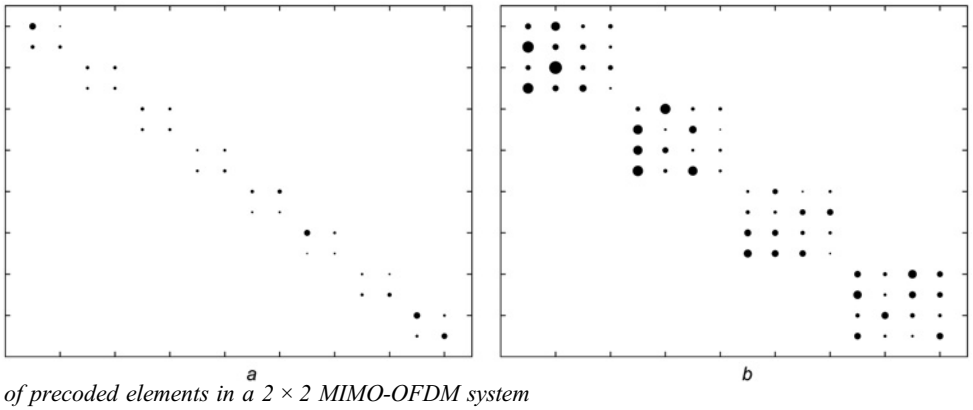

Fig. 3 *Amplitudes of precoded elements in a 2 × 2 MIMO-OFDM system*

The size of the dots is proportional to the amplitude of precoder coefficients. Only eight subcarriers are shown
a No subcarrier grouping
b Precoding with subcarrier grouping

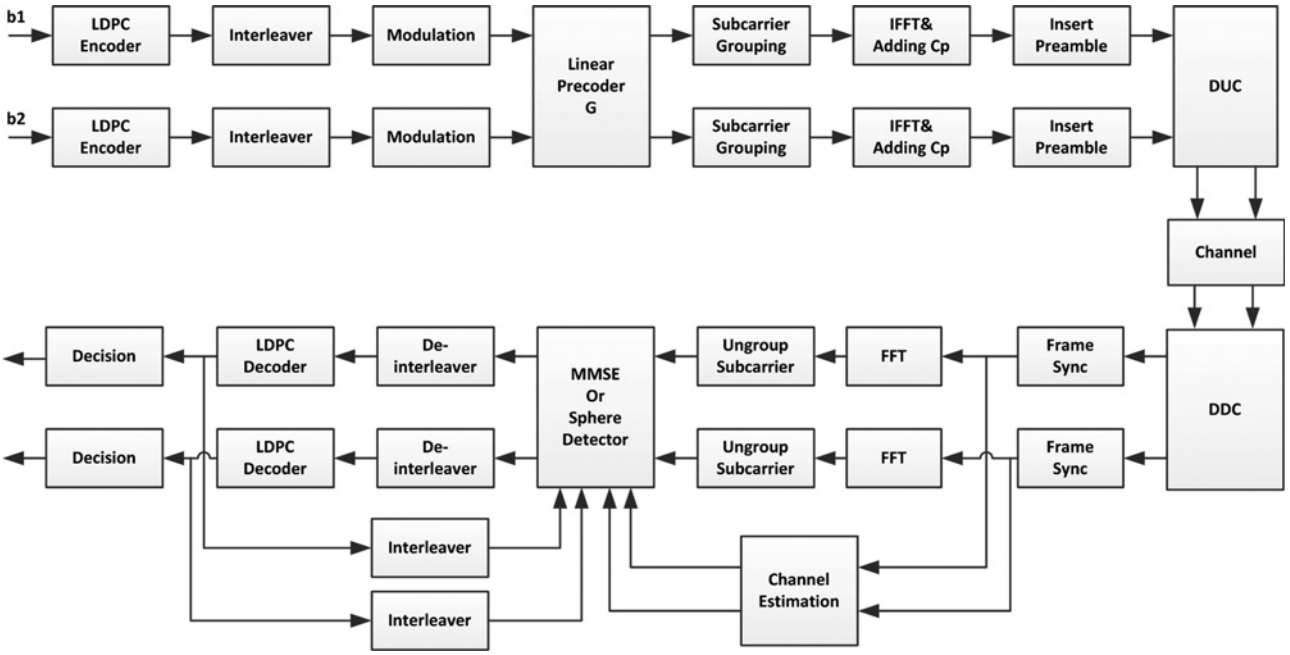

Fig. 4 *System diagram of 2 × 2 MIMO-OFDM system*

sequence at each transmitter antenna is a frame header for frame and symbol synchronisation. The two ***BPSK*** sequences are two different pseudo-random noise (PN) sequences generated by linear feedback shift registers with different initial seeds. The two preambles at each antenna in Fig. 5 serve as training sequences for channel estimation. Each preamble consists of a 256-symbol length Chu sequence [33] and a 128-symbol length cyclic prefix (CP). The CP length is chosen so that it is greater than the length of the channel impulse response (CIR). The preambles have the following structure [34, 35]

$$\begin{bmatrix} \text{Preamble 1} & \text{Preamble 2} \\ \text{Preamble 3} & \text{Preamble 4} \end{bmatrix} = \begin{bmatrix} S_{\text{chu}} & -S_{\text{chu}}^* \\ S_{\text{chu}} & S_{\text{chu}}^* \end{bmatrix} \quad (28)$$

where S_{chu} is a 256-symbol Chu sequence. Two OFDM data

doi: 10.1049/iet-com.2012.0731

Tx 1	BPSK Seq 1	Preamble 1		Preamble 2		Data Block 1		Data Block 2	
	144	128CP	256	128CP	256	128CP	2048	128CP	2048
Tx 2	BPSK Seq 2	Preamble 3		Preamble 4		Data Block 3		Data Block 4	
	144	128CP	256	128CP	256	128CP	2048	128CP	2048

Fig. 5 *Frame structure of MIMO-OFDM signaling*

blocks follow the preambles, and each data block consists of 2048 data symbols preceded by 128 symbols of CP.

As shown in Fig. 4, the data blocks at the transmitter are generated by two raw source bit streams $\boldsymbol{b}_1$ and $\boldsymbol{b}_2$ encoded by an LDPC encoder with 3/4 coding rate and codeword length of 2040 bits. We employ the LDPC channel codes specified by the latest WiMAX standard [36], which has also been realised in the software package in [37]. After LDPC encoding, each codeword is added eight bits of zeros at the end to form a data block of length 2048, which is then interleaved and modulated to symbols. The supported modulation schemes in our implementation are QPSK, ***8PSK***, or 16QAM.

Table 4 Description of key equipments

Function	Equipment
FPGA platform for Tx	Altera Stratix III FPGA Development kit w/daughter board
FPGA platform for Rx	Altera Stratix IV FPGA Development kit w/daughter board
receive antennas	Pharad's wearable antennas, BW-800-900-D
RF up-converter	NuWaves, RF2-3000UCV1
transmitter power amplifiers (optional)	RF Bay, MPA-10-40
receiver low noise amplifier (optional)	RF Bay, LNA-0915
RF down-converter	NuWaves, RF200-2500RV1
external clock for frequency reference	FS725 rubidium frequency standard

After precoding, the symbols of each stream are fed into a subcarrier grouper, which is discussed in Section 3. After the subcarrier grouping, each data block is converted to time domain signals by inverse fast Fourier transform (IFFT), followed by CP insertion and preamble insertion. The digital up converter (DUC) is used to up-sample the baseband signals and modulate them into the 17.5 MHz IF. The output of the DUC module is fed to the digital-to-analogue converter (DAC) directly.

At the receiver, the analogue-to-digital converter (ADC) bandpass sampling rate is 125 MHz and the IF is 70 MHz. The digital down converter (DDC) module down-samples the IF signals to baseband I and Q signals. At each receive antenna, the frame synchroniser captures the received frame based on the time domain correlations of the local PN sequence. After the start of the frame is located, the received preambles are used for channel estimation which uses frequency domain LS method [34, 35]. The received preambles are first converted to frequency domain with a 256-point FFT. For each subcarrier of the preamble, LS estimation is performed to obtain an initial estimation of a 2×2 channel matrix. Then we convert the estimated channel matrices to time domain with a 256-point IFFT and pass them through a rectangular window whose width is larger than the length of the CIR. Finally, we convert the windowed CIR to frequency domain channel response $\hat{\boldsymbol{H}}_i$ using a 2048-point FFT.

A turbo receiver is employed to iteratively exchange log-likelihood ratio (LLR) between the MIMO MMSE-IC soft detector [16, 17] and the LDPC channel decoder for each bit stream. Alternatively, the list FSD [18, 19] is also implemented. Since the soft MIMO detector group received

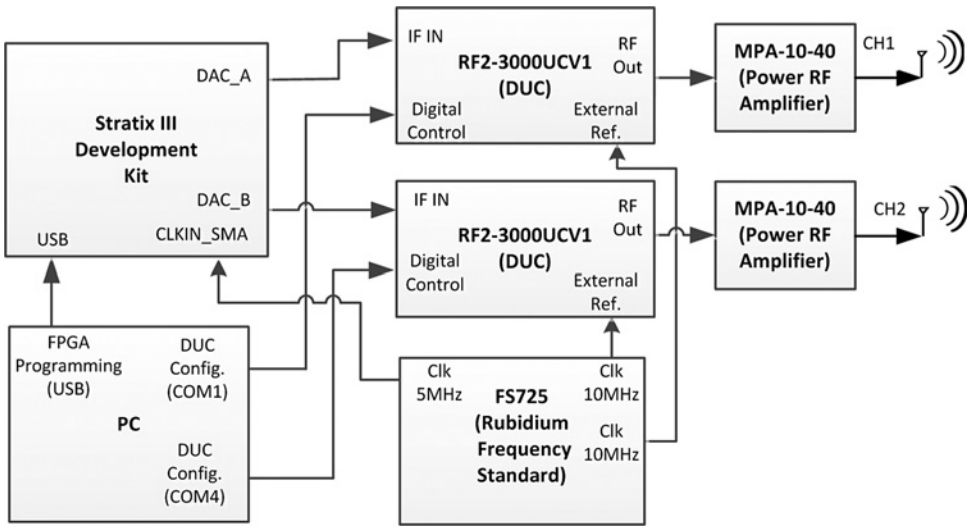

Fig. 6 *Transmitter setup architecture*

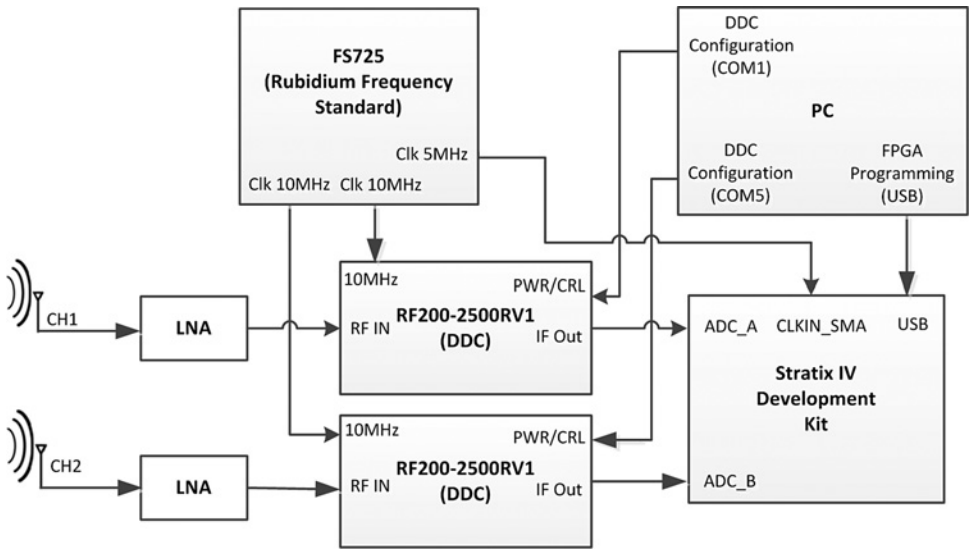

Fig. 7 *Receiver setup architecture*

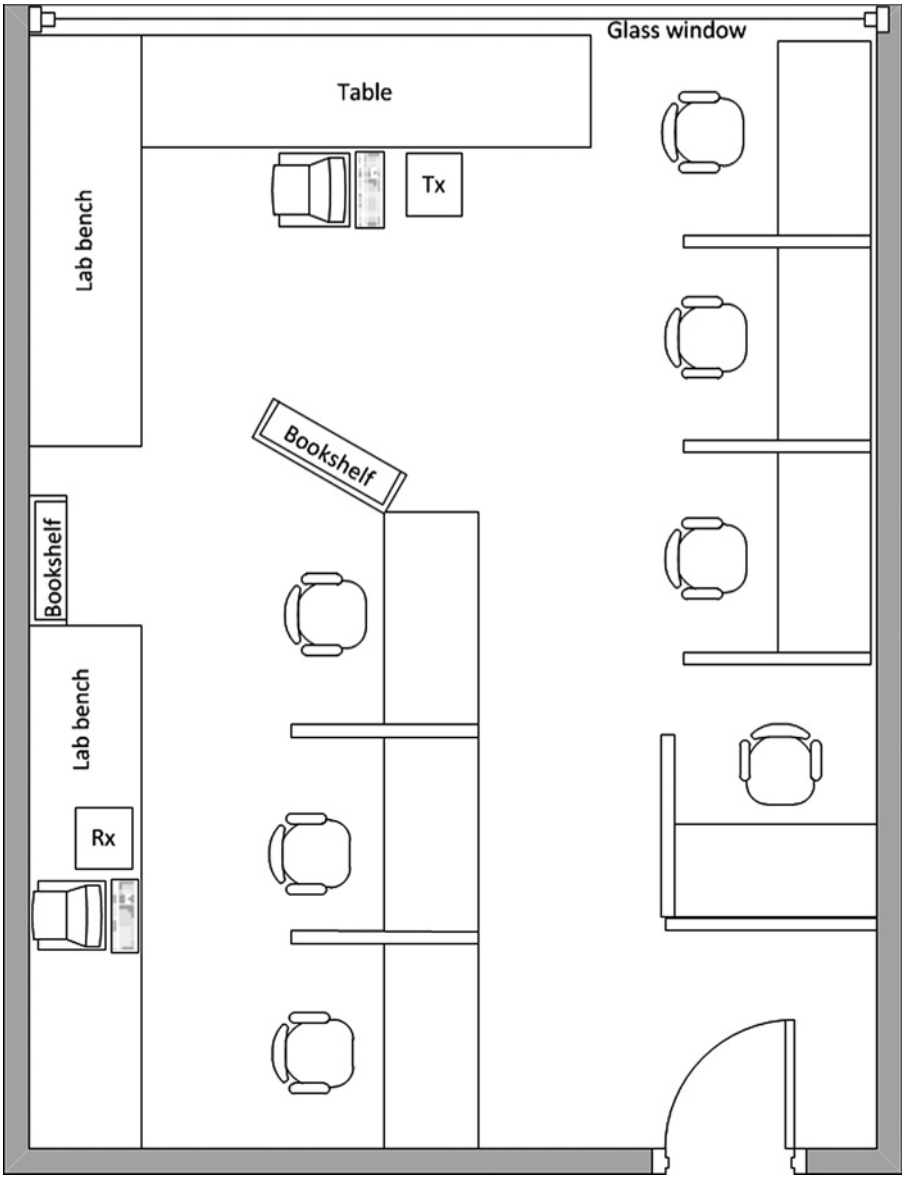

Fig. 8 *Floor plan of the indoor NLOS environment (9.1 m × 7.0 m)*

doi: 10.1049/iet-com.2012.0731

signals from two subcarriers to detect symbols, the effective channel matrices $\boldsymbol{H}_{ei} = \hat{\boldsymbol{H}}_i \boldsymbol{G}_i, \quad i = 1, 2, \ldots, 1024,$ are used in both MMSE-IC and FSD schemes. The MIMO detector generates extrinsic LLR, based on $\boldsymbol{y}_i$ and the *a priori* information from the LDPC channel decoders. The extrinsic information of MIMO detector is then interleaved and sent to the LDPC decoder as its *a priori* input. By employing soft channel decoding methods such as log domain sum-product algorithm [38], the LDPC decoder computes its extrinsic information as output, which is fed back to the MIMO detector as the *a priori* information. After two turbo iterations, hard decisions are made at the output of the LDPC decoder.

5 Testbed, experiment setup, and results

In this section, we present the setup of the MIMO-OFDM testbed and discuss the experiment results.

5.1 Testbed and experiment setup

The testbed was built using the equipment listed in Table 4. The baseband processing was implemented on Altera Stratix III FPGA development kits [39]. The FPGA-DSP development kit features Stratix III EP3SL150F1152 high-performance FPGA, and ADC/DAC daughter board. Baseband signal processing was implemented in Altera FPGA and daughter board. The detailed architecture setup of the transmitter and receiver are shown in Figs. 6 and 7.

In the transmitter shown in Fig. 6, we implemented the baseband modules and DUC in the Stratix III FPGA and utilised the DAC daughter board to convert two data streams to analog IF signals. At each stream of the transmitter, the IF signals were fed into the low pass filter SLP-50 with 50 MHz bandwidth to reduce the out of band noise. Then the NuWave RF2–3000UCV1 radio frequency (RF) up-converter was employed to up-convert the IF signal to 915 MHz RF signals. The MPA-10-40 RF was chosen for power amplification, before the signals being transmitted through wearable antennas. The computer was used to program the FPGA and to configure the RF up-converters. The transmit power can be adjusted manually by changing the attenuation level of the RF up-converter. The FS725 rubidium clock serve as an external reference clock for FPGA board and RF up-converters.

At the receiver side, the signals were received by antennas and then down-converted to 70 MHz IF signals by the RF front-end. The 2-channel 14-bit ADC daughter board was employed to convert analog signals into digital signals via bandpass sampling. The sampling frequency was also 125 MHz and the folded IF frequency was 55 MHz.

5.2 Field experiments

5.2.1 Procedures: Our experiments were conducted in three steps. Step 1 was channel acquisition without precoding. We transmitted packets using identity matrices as precoders, received the signals and estimated the channels. Step 2 was offline precoder design for all subcarriers based on the estimated channels. After the precoding matrices were computed at a fixed SNR, they were quantised and stored in read-only memories of the transmitter FPGA. Step 3 was performance verification with precoding. A particular precoding method was selected and multiple frames were transmitted with the assumption that the channels are static. We change the attenuation level of the RF upconverter at the transmitter to obtain different values of signal transmission power. Under a specific modulation scheme, we use the manual gain controller of the RF downconverter at the receiver side to adjust the spectra of the received signals. Experiment data was logged at the DDC output through Signal Tap II logic analyser of Quartus II and baseband receiver was implemented in MATLAB.

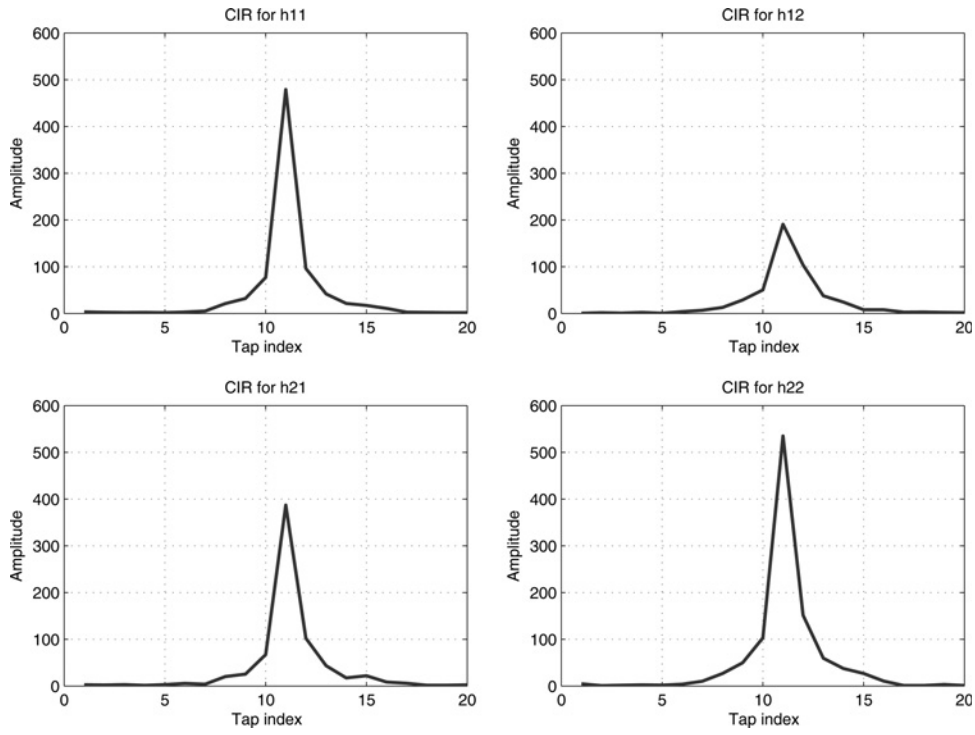

Fig. 9 *Estimated CIRs of indoor same room NLOS environment*

Table 5 BER results using list FSD for indoor same room NLOS experiments

Modulation	Tx attenuation, dB	Classic WF	Channel diagonalisation	Maximum diversity	Proposed method
QPSK	18	0.3896	0.3776	0.07614	0.00784
	16	0.3806	0.1003	0	0
	14	0.3578	0.05833	0	0
	10	0.3858	0	0	0
8PSK	18	0.4149	0.4419	0.2015	0.121
	16	0.4031	0.3425	0.08562	0.0488
	14	0.4116	0.2091	0.05403	0.03475
	10	0.3700	0.2170	0.009695	0.002505

5.2.2 Indoor same room NLOS: We conducted indoor NLOS experiments in Room 208 of the Emerson Electric Company Hall at the Missouri University of Science and Technology campus. The transmitter and receiver are located in the same room with dimensions of 9.1 m × 7.0 m. In addition, a metal bookshelf is placed between the transmitter and the receiver to block the line-of-sight communication path. The transmitter and receiver antennas are located at half of the height of the blocking bookshelf above the floor. The floor plan is shown in Fig. 8, where the ceiling is 2.6 m above floor.

5.2.3 Experiment results: Fig. 9 plots a snapshot of the estimated CIRs for the indoor same room NLOS environment, where h_{ij} represents the channel from jth transmit to ith receive antenna. It is observed that the length of all the channels are less than 20 taps. Our extensive experiments have shown similar characteristics of the CIRs. Therefore, the width of the time domain window for channel estimation are set to 20.

Table 5 lists BER results of using list FSD method for data processing. The experiments include different modulations for precoding schemes 1, 2 and 3 discussed in Section 2, and the proposed precoding method in Section 3. From the results of QPSK and ***8PSK*** shown in Table 5, it is seen that the proposed method achieved lowest BER among all the implemented precoding methods in our system. In addition, the maximum diversity outperformed the classic water-filling and channel diagonalisation. The performance gains of the proposed method and the maximum diversity over the other two schemes are due to the fact that these two approaches take into account the specific structure of finite-alphabet inputs and offer higher mutual information. Such observations from the experiments are similar to the simulation results in [14], which includes the optimal precoding and the maximum diversity methods with MAP detection. For the list FSD in our receiver, the node distribution [19] for QPSK was $\boldsymbol{n}_s = [1, 1, 4, 4]$, and the number of survival candidates to calculate LLR was $N_L = 16$. For ***8PSK***, the distribution was set to $\boldsymbol{n}_s = [1, 1, 8, 8]$ and 16 candidates with the minimum distances were used for LLR calculations.

We also compared the data processing results of using list FSD and soft MMSE detection. As an illustrative example, Table 6 lists BER results of maximum diversity precoding under different modulation schemes. The parameters of the list FSD detection method were the same asthose in Table 5. From Table 6, we find that the list FSD method achieved better performance than the MMSE detection method.

Table 6 Comparison of BER results using list FSD and MMSE detection

Modulation	Tx attenuation, dB	List FSD	MMSE
QPSK	18	0.07614	0.0949
	16	0	0.019
	14	0	0.0054
	10	0	0
8PSK	18	0.2015	0.1978
	16	0.08562	0.1047
	14	0.05403	0.0776
	10	0.009695	0.0149
16QAM	20	0.1839	0.1779
	18	0.09943	0.1111
	16	0.08194	0.0989
	14	0.02655	0.0645
	10	0.004657	0.0516

6 Conclusions

In this paper, a practical linear precoding method for MIMO-OFDM system has been proposed that simplifies the two-step algorithm maximising the lower bound of the mutual information with finite-alphabet inputs. The proposed algorithm achieves similar performance as the original two-step algorithm, but requires only 3–6% of the computational complexity; thus, making the precoding design feasible to practical systems.

The precoding design has been applied to a 2×2 MIMO-OFDM system with 2048 subcarriers by designing 1024 precoding matrices of size 4×4 based on the extended channel matrices that combine the 2×2 MIMO with two subcarriers. Experimental results of indoor NLOS experiments have shown that the proposed precoding method has achieved the lowest BER in comparison to maximum diversity, classic water-filling and channel diagonalisation methods.

7 Acknowledgments

The authors would like to thank Mr. Bing Han and Drs. Fei Ren and Huang Lou for their helps with the FPGA transceiver implementation and field experiments.

This work was supported in part by Office of Naval Research under Grant N00014-09-1-0011 and by National Science Foundation under Grants ECCS-0846486, CCF-0915846 and ECCS-1231848.

8 References

1 Cover, T.M., Thomas, J.A.: 'Elements of information theory' (Wiley, New York, 2006, 2nd edn.

2 Xin, Y., Wang, Z., Giannakis, G.B.: 'Space-time diversity systems based on linear constellation precoding', *IEEE Trans. Wirel. Commun.*, 2003, **2**, (1), pp. 294–309

3 Palomar, D.P., Cioffi, J., Lagunas, M.A.: 'Joint Tx–Rx beamforming design for multicarrier MIMO channels: a unified framework for

doi: 10.1049/iet-com.2012.0731

convex optimization', *IEEE Trans. Signal Process.*, 2003, **51**, (9), pp. 2381–2401
4 Palomar, D.P., Verdú, S.: 'Gradient of mutual information in linear vector Gaussian channels', *IEEE Trans. Inf. Theory*, 2006, **52**, (1), pp. 141–154
5 Lozano, A., Tulino, A.M., Verdú, S.: 'Optimum power allocation for parallel Gaussian channels with arbitrary input distributions', *IEEE Trans. Inf. Theory*, 2006, **52**, (7), pp. 3033–3051
6 Xiao, C., Zheng, Y.R.: 'On the mutual information and power allocation for vector Gaussian channels with finite discrete inputs'. Proc. IEEE Global Telecommunications Conf. (Globecom), New Orleans, USA, December 2008, pp. 1–5
7 Xiao, C., Zheng, Y.R.: 'Transmit precoding for MIMO systems with practical CSI and discrete-constellation inputs'. Proc. IEEE Int. Conf. on Communications (ICC), Dresden, Germany, June 2009, pp. 1–5
8 Payaró, M., Palomar, D.P.: 'On optimal precoding in linear vector Gaussian channels with arbitrary input distribution'. Proc. IEEE Int. Symp. on Information Theory, Seoul, Korea, June 2009, pp. 1085–1089
9 Lamarca, M.: 'Linear precoding for mutual information maximization in MIMO systems'. Proc. Sixth Int. Symp. on Wireless Communication Systems, Siena, Italy, 2009, pp. 26–30
10 Pérez-Cruz, F., Rodrigues, M.R.D., Verdú, S.: 'MIMO Gaussian channels with arbitrary inputs: optimal precoding and power allocation', *IEEE Trans. Inf. Theory*, 2010, **56**, (3), pp. 1070–1084
11 Xiao, C., Zheng, Y.R., Ding, Z.: 'Globally optimal linear precoders for finite alphabet signals over complex vector Gaussian channels', *IEEE Trans. Signal Process.*, 2011, **59**, (7), pp. 3301–3314
12 Wang, M., Xiao, C., Zeng, W.: 'Linear precoding for MIMO multiple access channels with finite discrete inputs', *IEEE Trans. Wireless Commun.*, 2011, **10**, (11), pp. 3934–3942
13 Zeng, W., Zheng, Y.R., Wang, M., Lu, J.: 'Linear precoding for relay networks: a perspective on finite-alphabet inputs', *IEEE Trans. Wirel. Commun.*, 2012, **11**, (3), pp. 1146–1157
14 Zeng, W., Xiao, C., Wang, M., Lu, J.: 'Linear precoding for finite-alphabet inputs over MIMO fading channels with statistical CSI', *IEEE Trans. Signal Process.*, 2012, **60**, (6), pp. 3134–3148
15 Hochwald, B., ten Brink, S.: 'Achieving near-capacity on a multiple-antenna channel', *IEEE Trans. Commun.*, 2003, **51**, (3), pp. 389–399
16 Boher, L., Rabineau, R., Helard, M.: 'An efficient MMSE equalizer implementation for 4×4 MIMO-OFDM systems in frequency selective fast varing channels'. Proc. IEEE Personal, Indoor and Mobile Radio Communications (PIMRC), Athens, Greece, September 2007, pp. 1–5
17 Boher, L., Rodrigue, R., Helard, M.: 'FPGA implementation of an iterative receiver for MIMO-OFDM Systems', *IEEE J. Sel. Areas Commun.*, 2008, **26**, (8), pp. 857–866
18 Barbero, L.G., Thompson, J.S.: 'Fixing the complexity of the sphere decoder for MIMO detection', *IEEE Trans. Wirel. Commun.*, 2008, **7**, (6), pp. 2131–2142
19 Barbero, L.G., Thompson, J.S.: 'Extending a fixed-complexity sphere decoder to obtain likelihood information for Turbo-MIMO systems', *IEEE Trans. Veh. Technol.*, 2008, **57**, (9), pp. 2804–2814
20 Sampath, H., Talwar, S., Tellado, J., Erceg, V., Paulraj, A.: 'A fourth-generation MIMO-OFDM broadband wireless system: design, performance, and field trial results', *IEEE Commun. Mag.*, 2002, **40**, (9), pp. 143–149
21 Dubuc, C., Starks, D., Creasy, T., Yong, H.: 'A MIMO-OFDM prototype for next-generation wireless WANs', *IEEE Commun. Mag.*, 2004, **42**, (12), pp. 82–87
22 van Zelst, A., Schenk, T.C.W.: 'Implementation of a MIMO OFDM based wireless LAN system', *IEEE Trans. Signal Process.*, 2004, **52**, (2), pp. 483–494
23 Yu, H., Kim, M., Choi, E., Jeion, T., Lee, S.: 'Design and prototype development of MIMO-OFDM for next generation wireless LAN', *IEEE Trans. Consum. Electron.*, 2005, **51**, (11), pp. 1134–1142
24 Haustein, T., Forck, A., Gäbler, H., Jungnickel, V., Schiffermüller, S.: 'Real-time signal processing for multiantenna systems: algorithms, optimization, and implementation on an experimental test-bed', *EURASIP J. Appl. Signal Process.*, 2006, Article ID 27 573, pp. 1–21
25 Haene, S., Perels, D., Burg, A.: 'A real-time 4-stream MIMO-OFDM transceiver: system design, FPGA implementation, and characterization', *IEEE J. Sel. Areas Commun.*, 2008, **26**, (8), pp. 877–889
26 Gómez-Calero, C., Navarrete, L.C., Haro, L., Martiínez, R.: 'A 2×2 MIMO DVB-T2 system: design, new channel estimation scheme and measurements with polarization diversity', *IEEE Trans. Broadcast.*, 2011, **57**, (6), pp. 195–203
27 Telatar, E.: 'Capacity of multi-antenna Gaussian channels', *Eur. Trans. Telecommun. ETT*, 1999, **10**, (11), pp. 585–596
28 Goldsmith, A.: 'Wireless communications' (Cambridge University Press, 2005) pp. 301
29 Zeng, W., Xiao, C., Lu, J.: 'A low-complexity design of linear precoding for MIMO channels with finite-alphabet inputs', *IEEE Wirel. Commun. Lett.*, 2012, **1**, (1), pp. 38–41
30 Yu, W., Cioffi, J.M.: 'Constant-power waterfilling: performance bound and low-complexity implementation', *IEEE Trans. Commun.*, 2006, **54**, (1), pp. 23–28
31 Xiao, C., Zheng, Y.R.: 'On the ergodic capacity of MIMO triply selective Rayleigh fading channels', *IEEE Trans. Wirel. Commun.*, 2008, **7**, (6), pp. 2272–2279
32 Xiao, C., Wu, J., Leong, S.Y., Zheng, Y.R., Letaief, K.B.: 'A discrete-time model for triply selective MIMO Rayleigh fading channels', *IEEE Trans. Wirel. Commun.*, 2004, **3**, (5), pp. 1678–1688
33 Chu, D.: 'Polyphase codes with good periodic correlation properties', *IEEE Trans. Inf. Theory*, 1972, **18**, (7), pp. 531–532
34 Mody, A.N., Stuber, G.L.: 'Receiver implementation for a MIMO OFDM system'. Proc. IEEE Global Communications Conf. (Globecom), Taipei, Taiwan, November 2002, pp. 716–720
35 Stuber, G.L., Barry, J., McLaughlin, S., Li, Y., Ingram, M.A., Pratt, T.: 'Broadband MIMO-OFDM wireless communications', *Proc. IEEE*, 2004, **92**, (2), pp. 271–294
36 *Part 16:Air Interface for Broadband Wireless Access Systems*, IEEE Std 802.16^{TM}-2009, May. 2009
37 Valenti, M.: The Coded Modulation Library, http://www.iterativesolutions.com
38 Hu, X.Y., Eleftherious, E., Arnold, D.M., Dholakia, A.: 'Efficient implementations of the sum-product algorithm for decodng LDPC codes'. Proc. IEEE Global Telecommunications Conf. (Globecom), San Antonio, TX, USA, November 2001, pp. 1036–1036E
39 Altera. *Stratix III 3SL150 development kit reference manual* [Online]. Available: http://www.altera.com/products/devkits/altera/kit-siii-host.html